CATALYTIC REACTIONS OF TRANSITION METAL CLUSTERS AND SURFACES FROM AB-INITIO THEORY
–Cluster and Dipped Adcluster Model Studies Combined with the SAC/SAC-CI Method–

H. Nakatsuji, H. Nakai, and M. Hada

Department of Synthetic Chemistry
Faculty of Engineering
Kyoto University, Kyoto, Japan

ABSTRACT. Reactions of transition-metal clusters are of considrable interests by themselves and from an analogy to surface catalytic reactions. We first review here our ab-initio theoretical studies on the reactions of small metal clusters with a hydrogen molecule. The clusters investigated are palladium, platinum, and ZnO. We also investgate the hydrogenation reaction of acetylene catalyzed by palladium. We study the energetics, mechanism, cluster-size dependence, surface stability, etc. and propose a molecular beam study for confirming the results. We next consider the case in which the electron transfer between an admolecule and a surface is important. We propose dipped adcluster model (DAM) in which adcluster (admolecule + cluster) is dipped onto the electron bath of the solid metal and an equilibrium is established for the electron exchanges. The role of the electrostatic image force is investigated. Electron correlations, electron transfers, and participations of lower excited states which are important for surface electronic processes are described by the SAC/SAC-CI method. We apply these methods to oxygen chemisorptions on palladium and silver surfaces.

1. INTRODUCTION

For theoretically studying catalytic reactions on a metal surface, the first question is "how do we describe molecule-surface interaction". It involves the interaction between finite and infinite systems so that a modelling is necessary for an adequate description of the system. In this review article, we consider two models; cluster model and dipped adcluster model.[1]

Cluster model is based on the locality of the interaction between an admolecule and a surface: namely the admolecule can interact directly with only a few atoms of a surface. We apply this model to hydrogen chemisorptions on Pd, Pt, and ZnO surfaces.[2-4] We then study the hydrogenation reaction of acetylene on a Pd surface.[5] Strictly speaking, these studies are actually for the reactions of the small metal clusters with hydrogen and acetylene.

When electron transfer between admolecule and surface is important, the clus-

D. R. Salahub and N. Russo (eds.), Metal-Ligand Interactions: from Atoms, to Clusters, to Surfaces, 251–285.

ter model may be inadequate. In such a case we propose a model[1] in which the adcluster, a combined system of the cluster and admolecule, is dipped onto the free electron bath of a bulk metal and an equilibrium is established for electron exchanges between them. This model is called dipped adcluster model (DAM) and applied to the study of oxygen chemisorptions on Pd and Ag surfaces.[1,6]

Electron correlations are very important for metal cluster and surface electronic processes. We very often deal with transition metals. Metal clusters and surfaces have many dangling bonds, so that they have many lower excited states which are sometimes involved in catalytic processes. Electron transfer is often important in such processes. Therefore, a reliable and efficient method for dealing with such electronic processes is necessary. We here use the SAC (symmetry adapted cluster)/SAC-CI method for groud, excited, ionized, and electron attached states[7-10] for describing electron correlations in surface lower states and electron transferred states. Since the review article on the SAC/SAC-CI method is written separately,[10] we do not explain it here.

We review in this article our ab-initio theoretical studies for the reactions of hydrogen molecule with small Pd and Pt clusters[2,3] and the hydrogenation reaction of acetylene on palladium.[5] The reaction modes are considerably different between these two metals. We then investigate the hydrogen chemisorption on a semi-conductor surface, ZnO.[4] The electronic mechanism is very different from that on a metal surface. We next review an idea of the dipped adcluster model for chemisorptions and catalytic reactions involving electron transfer between admolecules and surfaces,[1] and apply it to oxygen chemisorptions on palladium[1] and silver surfaces.[6]

The basis sets of calculations are as follows. For Pd, Pt, and Ag atoms, the contracted [3s2p2d] sets are used and the Kr and Xe cores are replaced by the relativistic effective core potential (ECP).[11] For Zn, the [2s2p2d] CGTO's are used and the Ar core is replaced by the ECP.[11] For hydrogen, we use the [2s] set of Huzinaga-Dunning,[12] and for carbon the 4-31G set. We have added the first derivative bases for Hand C so that the Hellmann-Feynman theorem is approximately satisfied for the forces acting on the hydrogens and carbons.[13] For oxygen, the [4s2p] CGTO plus anion s,p bases[14] and d-polarization functions are used for the calculations with silver and in ZnO, and 4-31 G set for those with palladium. Most Hartree-Fock calculations are done with the use of the program GAMESS.[15]

2. HYDROGEN CHEMISORPTION ON PALLADIUM

We first study the interaction of a hydrogen molecule with a Pd atom. The ground $^1S(d^{10})$ state of the Pd atom shows an affinity to the H_2 molecule, but does not cleavage the H-H bond. The equilibrium geometry is an equilateral triangle with the H-H distance of 0.768 Å, very close to that of the free molecule 0.741 Å and the Pd-H distance of 1.898 Å. The excited states, $^{1,3}D(d^9s^1)$ are repulsive.

We next consider an approach of H_2 to Pd_2 as illustrated in Figure 1. This side-on orientation of H_2 was shown to be most stable. The Pd-Pd distance is fixed to 2.7511 Å, the bulk fcc crystal structure.[16] In Figure 1, we show the potential curves of H_2 at several Pd_2-H_2 separations, R. They were calculated by the CAS-SCF method.[17] When R is larger than 2.5 Å, the potential of H_2 is essentially the

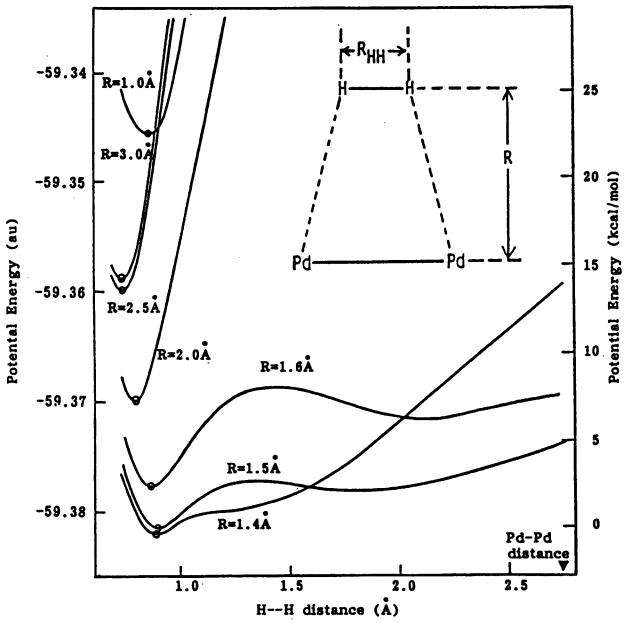

Figure 1. Potential curves for the H-H stretching of the Pd_2-H_2 system at different Pd_2-H_2 separations (CAS-SCF method).

same as that of the free molecule. When H_2 approaches Pd_2 up to R = 2.0 Å, the H-H distance becomes longer but the potential is still very sharp. However, at R = 1.4 ~ 1.6 Å, the potential curve suddenly (catastrophically) becomes very flat for an elongation of the H-H distance. At R = 1.6 Å, a double-well potential appears, and at R = 1.5 Å, the system becomes considerably more stable than that at R = 1.6 Å. Here, the second minimum appears at R(H-H) = 1.75 Å, besides the first minimum at R(H-H) = 0.847 Å. At R = 1.4 Å, the first minimum is more stabilized than that at R = 1.5 Å, but the second minimum disappears. When the H_2 molecule further approaches Pd_2 up to R = 1.0 Å, the system becomes very much unstable. Thus, a stable adsorption of the H_2 molecule seems to occur at about 1.5 Å, from the Pd surface. The calculated heat of adsorption is about 15 kcal/mol which is smaller than the experimental value, 20.8 ~ 24.4 kcal/mol, for the bulk Pd surface.[18]

In order to obtain more reliable potential curves of H_2 interacting with Pd_2 at R = 1.5 Å, we calculated the potential curve of the ground state by the SAC method, and those of the singlet and triplet excited states by the SAC-CI method. Figure 2 shows the results. In the ground-state curve, we clearly see two potential minima. The minimum at R(H-H) = ~ 0.89 Å, corresponds to the molecular adsorption form, and that at R(H-H) = ~ 2.1 Å, corresponds to the dissociative form. The dissociative form is more stable than the molecular form by 2.2 kcal/mol and the barrier height is 5.6 kcal/mol. However, since the motion along the metal surface was not energetically optimized, the actual barrier could be smaller. We note that at the second minimum, the Pd-H distance is ~ 1.5 Å, which is close to the experimental internuclear distance of a free PdH molecule, 1.529 Å.[19] Thus, the H_2 molecule with a binding energy of

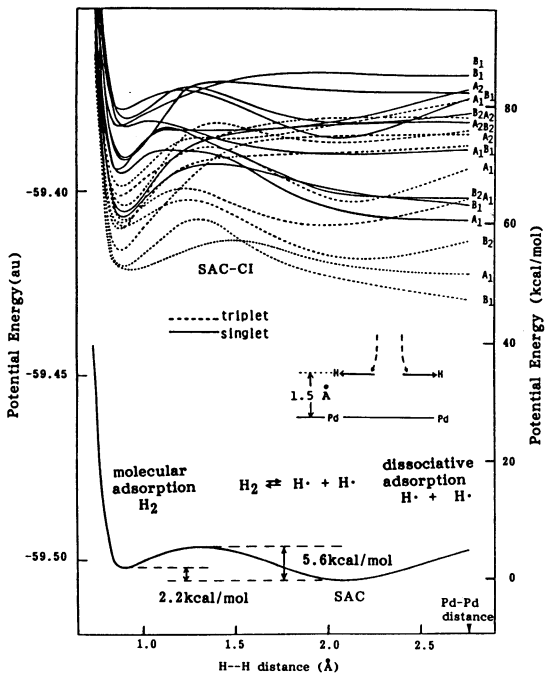

Figure 2. Potential energy curves of the ground and excited states of the Pd_2-H_2 system as a function of the H-H distance of the H_2 molecule 1.5 Å from the Pd_2 fragment (SAC and SAC-CI methods).

about 104 kcal/mol is dissociated, with almost no barrier, into two atomic hydrogens on the Pd_2 "surface", like on an extended surface.

From Figure 2, we see that the excited states of the Pd_2-H_2 system are well separated from the ground state, throughout the process, by more than 50 kcal/mol. There is almost no chance for the excited states to participate in the dissociative process. Therefore, the mechanism of the dissociative adsorption on the Pd surface is different from that proposed for a Ni surface by Melius et al.[20]

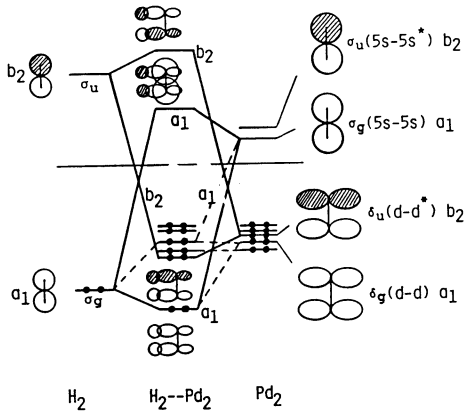

Figure 3. Schematic orbital correlation diagram for the interaction of H_2 and Pd_2.

Then, by what mechanism does the Pd_2 show such a catalytic ability ? Figure 3 shows a schematic orbital correlation diagram of the Pd_2-H_2 system. The left-hand side is the MO's of H_2, the right-hand side is the valence MO's of Pd_2, and the center is for the Pd_2-H_2 system. Two interactions are important. One is the electron transfer from the δ_u(d-d*)MO of Pd_2 to the antibonding MO of H_2. This transfer works to weaken the H-H bond. The other is the electron back-transfer from the bonding MO of H_2 to the bonding σ_g (5s-5s)MO of Pd_2. This back-transfer also works to weaken the H-H bond. These interactions increase as the H_2 approaches the Pd_2, and finally lead to a cleavage of the H-H bond. Other implications of this diagram are that the d electrons are important in the newly formed Pd-H bond and that the Pd-Pd bond is not weakened (rather strengthened) by the adsorption of H_2.

The last point is because, on the Pd_2 side, the electron flows out from the antibonding δ_u MO and flows into the bonding σ_g MO, resulting in a net increase in the Pd-Pd bond order. This aspect seems to be important in relation to the stability of the catalyst, implying that the Pd atom is not exfoliated as a PdH molecule from the metal surface. We note that these $4d_\delta$ and 5s AO's constitute the so-called "dangling" bonds of the metal surface. This mechanism may be simplified as the bond alternation mechanism shown below.

We have obtained a density profile which confirms such a bond alternation.

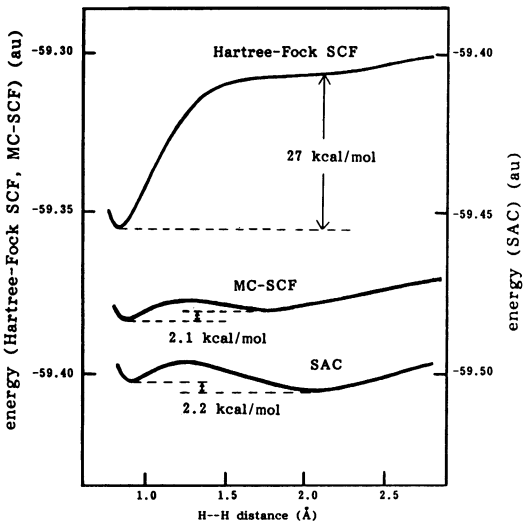

Figure 4. Potential energy curves for the H-H separation of the Pd_2-H_2 system with the Pd_2-H_2 distance at 1.5 Å calculated by the Hartree-Fock, CAS-SCF, and SAC methods.

We must say that the electron correlation is an origin of the dissociative adsorption, since it can not be explained even qualitatively without including the electron correlation. Figure 4 shows the potential curves of H_2, as that shown in Figure 2, calculated by the Hartree-Fock, CAS-SCF, and SAC/SAC-CI methods. We see

that the dissociative state is more stable than the molecular state only when the SAC method is used. The Hartree-Fock result fails to predict the existence of the dissociative adsorption state.

We have further shown that the existence of molecular and dissociative states of H_2 on a Pd surface explains the irreversibility in the observation of the photoemission spectra of the H-exposed Pd surface.[21-23] The discussions are found in ref. 2.

3. HYDROGENATION OF ACETYLENE ON PALLADIUM

As we have thus obtained dissociatively adsorbed hydrogens on the Pd_2 cluster on a purely theoretical ground, we investigate here the activity of this system for the hydrogenation reaction. We have chosen acetylene as a reactant because the catalytic reaction

$$C_2H_2 + H_2 \rightarrow C_2H_4 \quad (1)$$

is useful in chemical industry for converting acetylene included as impurities in ethylene gas. Palladium is a good catalyst of this reaction and shows the selectivity which is practically very important.[24] Namely, as far as acetylene exists in the mixture, it is hydrogenated selectively to ethylene, and ethane is not formed. Another reason we have chosen this reaction is that it is typically a symmetry-forbidden reaction.[25,26] Without an existence of the catalyst the barrier of this reaction is too high to occur smoothly. Then, an actual occurrence of this reaction on a palladium surface should be due to the catalytic activity of palladium. We want to know the electronic origin of this catalytic activity.

We consider here two modes of the reaction. One is that acetylene in a gas phase or in a Van der Waals layer of the catalyst reacts with the hydrogen molecule dissociatively adsorbed on palladium. This pathway is called Eley-Rideal (ER) mode. This mode is suitable for investigating the reactivity of the hydrogens dissociatively adsorbed on Pd_2. Experimentally this mode is not necessarily realistic, since acetylene is more easily adsorbed on palladium than hydrogen.[27] However, this reaction mode would become realistic when molecular beam experiment is undertaken. It would give valuable information on the reactivity of hydrogens adsorbed on a metal cluster.

Another mode we investigate is the surface reaction in which hydrogen dissociatively adsorbed on palladium attacks acetylene also adsorbed on the surface. This mode is called Langmuir-Hinshelwood (LH) mode. This mode is experimentally natural,[27] but theoretically more difficult than the ER mode, because of the larger freedom in the reaction pathway.

3.1. Eley-Rideal Mode

The assumed pathway of the ER mode and the forces acting on the carbons and hydrogens of the system during the reaction are shown in Figure 5. This force is calculated by using the Hellmann-Feynman theorem, which is satisfied since the basis sets for C and H include derivative bases.[13]

As seen from Figure 5, the system is repulsive in the beginning of the reaction, showing an existence of potential barrier. This is seen for the positions 1 and 2 of Figure 5. The hydrogens adsorbed on Pd_2 and acetylene are repulsive to each other.

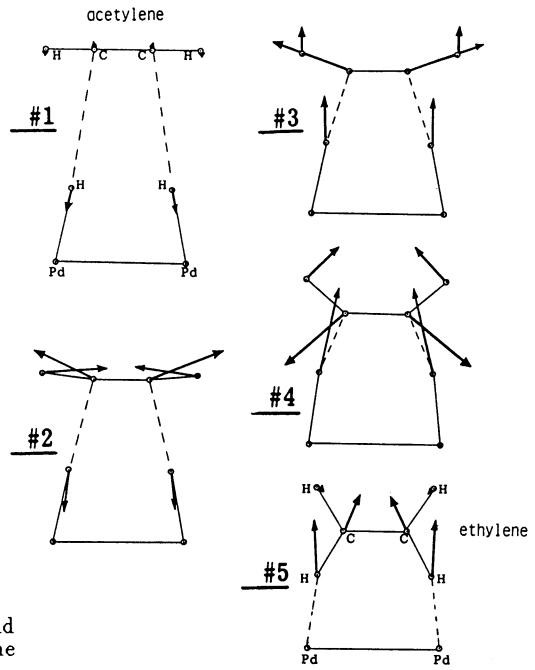

Figure 5. Force acting on the carbons and hydrogens during the Eley-Rideal mode of the reaction.

In the form 3, the forces acting on carbons are still repulsive, but the forces acting on the hydrogens on Pd_2 are attractive and the terminal hydrogens of acetylene feel the bending force. In the form 4, all of the forces acting on hydrogens and carbons work to accelerate the reaction. In the form 5, ethylene is formed and the force works to push out the product ethylene out from the Pd_2. Therefore, the ethylene is released automatically from the catalytic 'surface' of Pd_2. The active site of Pd_2 thus generated again adsorbs H_2 and enter into the catalytic cycle of the reaction. We should note that though ethylene is attractive to palladium when its π-orbital attacks the surface, it is repulsive in the form shown in 5 of Figure 5.

The corresponding potential energy curve for the reaction is shown in Figure 6. It also shows the potential curves for the same reaction without Pd_2. The curve starting from the level, C_2H_2 + H_2(2.1 Å), is the potential curve of the system entirely same as that shown in Figure 5 except for the non-existence of the Pd_2. Another sharp curve is also without Pd_2 starting from C_2H_2 and molecular hydrogen (R(H-H) = 0.74 Å).

The barrier of the reaction with an existence of Pd_2 is about 32 kcal/mol with respect to the free system. It is much smaller than that of the same reaction without Pd_2, which is as large as 138 kcal/mol due to the symmetry forbidden nature of the reaction. When ethylene is formed on Pd_2, it is repelled out automatically from the surface, since there, C_2H_4 and Pd_2 are coplanar so that the system is more unstable than the free system by 22 kcal/mol. The Pd_2 fragment thus generated again adsorbs H_2 and enters again into the reaction cycle. This is the catalytic cycle of the hydrogenation reaction in the Eley-Rideal mode involving Pd_2 as a catalyst.

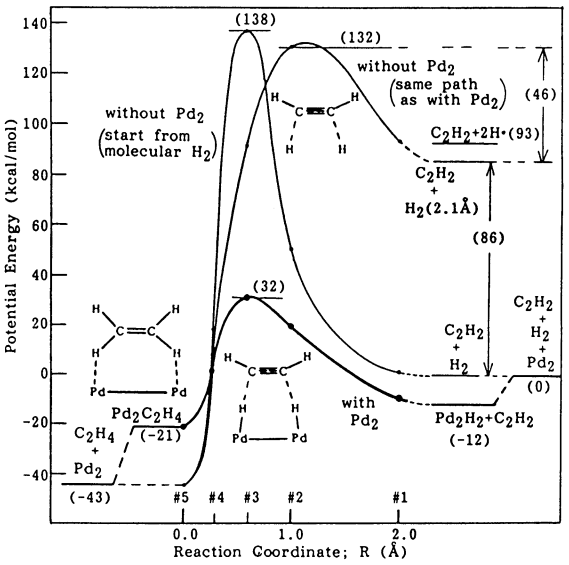

Figure 6. Potential energy curves for the hydrogenation reaction of acetylene with and without Pd_2. For the reaction without Pd_2, the steep curve on the left-hand side corresponds to the path starting from C_2H_2 and molecular hydrogen, and the curve on the right-hand side corresponds to the same pathway as that in Figure 5 except for the non-existence of the Pd_2. The numbers in the parentheses show relative energies in kcal/mol obtained by the CAS-SCF method.

When we start from C_2H_2 and two almost atomic hydrogens with the H-H distance of 2.1 Å, the H-H distance of the dissociatively adsorbed hydrogen on Pd_2, the barrier is about 46 kcal/mol, which is almost the same as the barrier 44 kcal/mol for the curve with Pd_2. The slopes of the two curves up to the transition states are also similar. This result implies two facts. First, the most important step, energetically, in this catalytic process is the dissociative adsorption of H_2 on a palladium surface. Second, the hydrogen dissociatively adsorbed on Pd_2 is essentially as reactive as a free atomic hydrogen, despite of the existence of the Pd-H bonds on the surface. This is indeed surprising and shows the catalytic activity of palladium in the second hydrogenation step.

3.2. Langmuir-Hinshelwood Mode

We next consider the Langmuir-Hinshelwood (LH) mode in which the olefin adsorbed on a metal surface is attacked by hydrogen also adsorbed on the surface.

Figure 7 shows the assumed pathway for the two step LH mode involving vinyl radical as a surface intermediate. Figure 8 shows the potential energy diagram for this reaction mode. The barrier is only 7 kcal/mol relative to the separated system. Afterwards, the reaction proceeds smoothly to form vinyl radical adsorbed on Pd_2, which is more stable than the separated system, $Pd_2 + C_2H_3$, by 7 kcal/mol. Therefore, the vinyl radical remains on the surface and receives second attack of the surface hydrogen to form ethylene. In this final product form, ethylene is coplanar with Pd_2 so that it is repelled automatically from the surface. This is the completion of the catalytic cycle. The naked site of palladium thus released adsorbs acetylene and hydrogen and enters again into the cycle. Thus, the two step LH mode involving vinyl radical as a surface intermediate is favorable as the mode of the hydrogenation

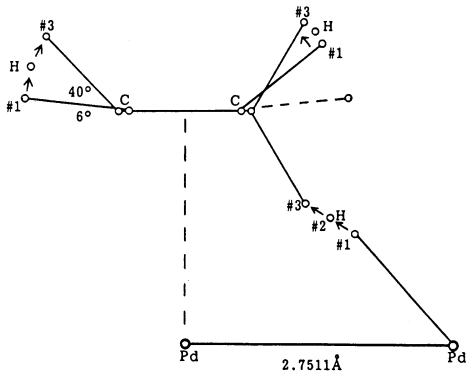

Figure 7. Assumed reaction pathways in the Langmuir-Hinshelwood mode. The Pd-Pd and Pd-C_2 distances are fixed throughout the reaction.

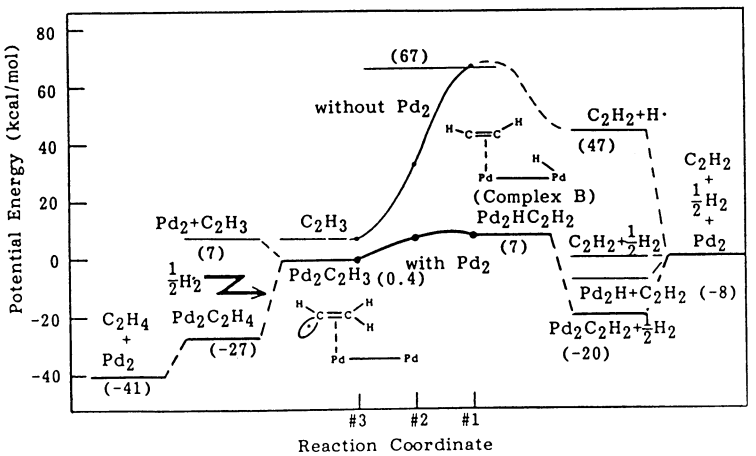

Figure 8. Energetics for the hydrogenation reaction of acetylene in the Langmuir-Hinshelwood mode. The coordinates 1 ~ 3 are shown in Figure 7. Energetics for the same pathway without Pd_2 is also shown. The numbers in parentheses show relative energies in kcal/mol.

reaction. This result agrees with the experimental observations.[27]

3.3. Selectivity in the Hydrogenation Reaction

Activity and selectivity are two major roles of catalyst. We explain here the selectivity of the palladium catalyst. It is summarized as follows. (1) Hydrogenation of ethylene does not occur until all acetylene impurities are converted to ethylene. (2) Ethane is generated only scarcely from acetylene. This selectivity occurs even though palladium is a better catalyst for the hydrogenation of ethylene.

A possible explanation based on the present calculation is as follows. For the first selectivity, the origin is that the heat of adsorption is larger for acetylene than for ethylene as observed experimentally.[27] Further, the sticking probability of acetylene

is larger than that of ethylene because acetylene has active π orbitals in all angles around the C-C axis but ethylene has the π orbital only in the plane perpendicular to the molecular plane. The second selectivity is due to the fact that the ethylene produced by the hydrogenation reaction of acetylene is coplanar with the active palladium atoms, so that, ethylene is repelled from the surface and released out automatically from the reaction cycle.

3.4. Proposed Molecular Beam Experiment

We propose here molecular beam experiments of the palladium clusters Pt_n ($n \geq 2$) as shown in Figure 9. When the beam of the Pd_n cluster is introduced through H_2 gas, it will chemisorb hydrogen molecule and the product beam $Pt_n(H_2)_m$ will come out, where H_2 is dissociatively adsorbed on the Pt_n cluster. When this beam is further introduced through acetylene gas at some temperature, it will be hydrogenated by the Eley-Rideal mechanism and ethylene will be generated. The acetylene gas will then become a mixture of ethylene and acetylene gases. The bare palladium sites produced may adsorb acetylene, but if the speed of the beam or the length of the acetylene tank is well regulated, we may get a bare palladium beam, which may be put again into the hydrogen gas. This is a cycle of the catalytic reaction with the use of the molecular beam as a catalyst.

Crossed molecular beam experiment shown below would give more detailed information on the dynamics of the reaction. The difference from the experiment shown above is that basically only one H_2 molecule will be chemisorbed on the Pd_n cluster and also only one acetylene molecule will attack this Pd_nH_2 cluster. Therefore when n is large, both ER and LH modes would occur on the cluster surface, giving rise to different behaviors in the product beams.

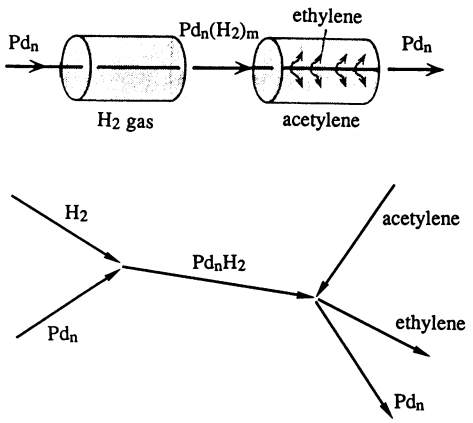

Figure 9. Proposed molecular beam experiments.

4. REACTIONS OF A HYDROGEN MOLECULE WITH SMALL PLATINUM CLUSTERS

We study here reactions of a hydrogen molecule with small platinum clusters Pt_n (n = 1,2,3) by ab initio methods. This provides a cluster model study for hydrogen chemisorption on a Pt surface.

4.1. Pt-H_2 System

We first examine side-on, on-top approach of a hydrogen molecule to a Pt atom. The definition of the reaction path is shown in Figure 10 and the accounts are found in ref. 3. In the Pt-H_2 system, only the central Pt atom (denoted as Pt_a) is considered.

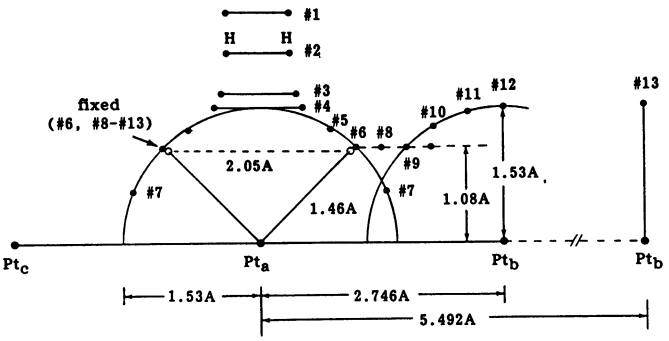

Figure 10. Reaction path for the Pt_n-H_2 (n = 1,2,3) system and the most stable geometry for the Pt-H_2 system shown by the open circles.

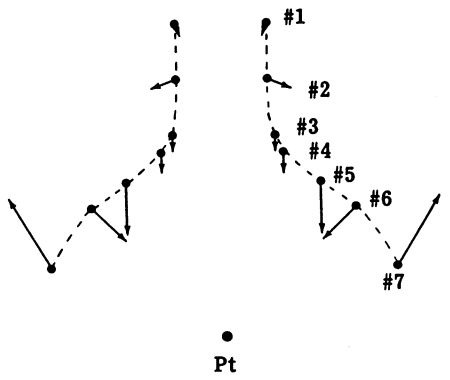

Figure 11. Forces acting on the H atoms in the Pt-H_2 system along the reaction path shown in Figure 10.

Figure 11 is a display of the forces acting on the H atom of the Pt-H_2 system calculted by the Hartree-Fock method for the $^1A_1$ state. At all the points, #1 ~ #6, the H atoms are attracted by the Pt atom. At the point #2, the H_2 molecule experiences the forces which act to elongate the H-H distance. At the points #3 ~ #5, that force is zero because the H-H distance has been optimized. At the point #7, the H atoms are repelled by the Pt atom. The optimized position of H_2 (open circles, Figure 10) is a little bit inside of the position #6, as indicated from the force.

The potential energy curves of the Pt-H_2 system calculated by the SAC/SAC-CI method are shown in Figure 12. The left-hand side (Figure 12a) is without the spin-orbit coupling effect and the right-hand side (Figure 12b) is with the spin-orbit coupling. All the triplet states arising from the ground state (^3D) of the Pt atom show large energy barriers of more than 16 kcal/mol (B_1, A_2, and B_2 states) with the stabilization energies less than 10 kcal/mol (B_2 state). Only the $^1A_1$ state, which originates from the excited ^1S state of the Pt atom, is very attractive. The calculated

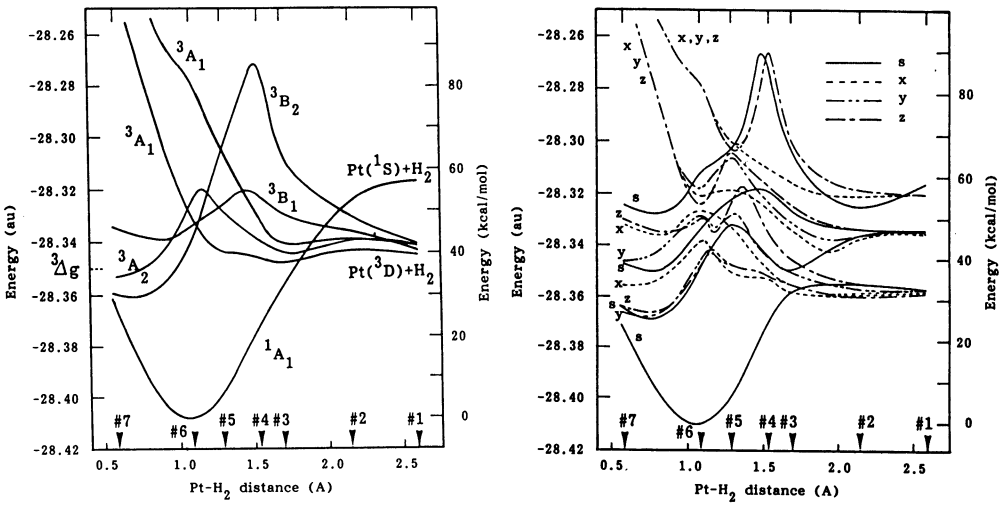

(a)without spin orbit coupling (b)with spin orbit coupling

Figure 12. Potential energy curves of the ground and excited states of the Pt-H_2 system in the side-on, on-top approach calculated by the SAC/SAC-CI method.

stabilization energy of the $^1A_1$ state, relative to the dissociation limit of Pt(^{3}D) + H_2, is about 40 kcal/mol, which is larger than the experimental heat of adsorption, 26 kcal/mol.[28] Thus, even a single Pt atom leads to a dissociative adsorption of a H_2 molecule. The catalytically active state for this adsorption is not the ground state, but the excited ^{1}S state of the Pt atom. When we consider spin-orbit interactions, we get the potential curves shown in Figure 12b. The potential well of the ground state at #5 and #6 geometries dissociates smoothly to the essentially ^{3}D state of Pt and a H_2 molecule. The heat of adsorption is calculated as 32.0 kcal/mol which is closer to the experimental value of 26 kcal/mol than that calculated from Figure 12a. On the basis of the present calculations, only the dissociative adsorption state is realized. The molecular adsorption state seems not to exist in contrast to the palladium case.

Next we analyze the electronic mechanism of the reaction. There are two important orbital interactions between H_2 and Pt as shown in Figure 13. At an early stage of the interaction, the electron transfer from the σ_g orbital of H_2 to the 6s orbital of the Pt atom is important. To accelerate the cleavage of the H-H bond, electron back-transfer from the d_{yz} orbital of the Pt atom to the σ_u orbital of H_2 is important. As the reaction proceeds, the electronic configuration of the Pt atom changes from d^{10} to a mixture of d^9s^1 and d^8s^2. As the Pt atom prefers the d^9s^1 and d^8s^2 configurations by 17.5 kcal/mol and 15.2 kcal/mol, respectively, to the d^{10} configuration,[29] this reaction proceeds very smoothly to dissociate completely the H_2 molecule. By contrast, as the Pd atom prefers the d^{10} configuration by 17.5 kcal/mol to the d^9s^1 configuration,[29] the dissociative adsorption by a single Pd atom does not occur, though it occurs smoothly on the Pd_2 cluster, as shown in the previous

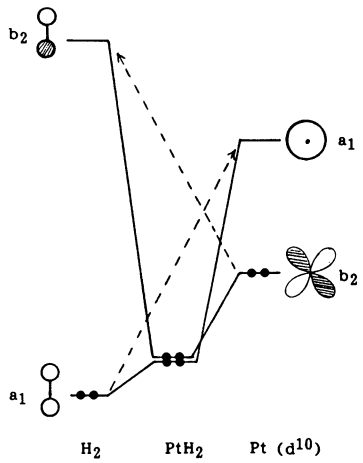

Figure 13. Orbital correlation diagram for the Pt-H_2 system.

section.

4.2. Pt_2-H_2 System

Here we consider the adsorption process of a hydrogen molecule on Pt_2 cluster. New aspects here are the migration process of a hydrogen atom on a Pt surface and the stability of the Pt-Pt bond during the catalytic process. The reaction path is shown in Figure 10. The metal atoms considered here are Pt_a and Pt_b, with the Pt-Pt distance being fixed at 2.746 Å.[16] The points #1 ~ #6 are the same as those described for the Pt-H_2 system. After reaching the position #6, which is very close to the optimized geometry of the Pt-H_2 system, the surface migration of the dissociated H atom is considered. The H atom on the left-hand side is fixed at this geometry and only the H atom on the right-hand side is moved from #6 to #12. This is the migration process of a hydrogen atom from Pt_a to Pt_b.

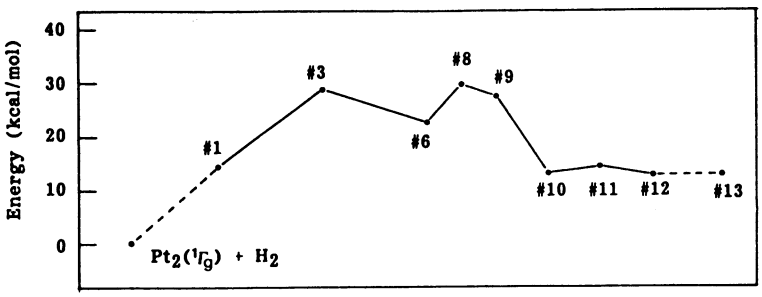

Figure 14. Potential energy diagram of the singlet ground state of the Pt_2-H_2 system calculated by the CAS-SCF method.

Figure 14 shows the energetics for the adsorption and migration processes of H_2 on Pt_2. The H_2 molecule must overcome a high barrier of 27.7 kcal/mol on going from the free system to point #3. Even after reaching point #6, the system is not

stabilized relative to the free system. This is very different from the Pt-H_2 system. Further, as the right H migrates on the Pt_2 surface from point #6 to #10, the energy of the system is lowered by about 15 kcal/mol, with the barrier of about 8 kcal/mol. Points #10 ~ #12 have almost the same energy. The adsorption energy calculated for this system is -12 kcal/mol which is the energy difference between #10 and the free system, $Pt_2(^1\Gamma_g)$ + H_2. Thus all of the processes considered for this system prove to be a game at an energy level higher than the free Pt_2 + H_2 system. This implies that the dissociative adsorption reaction of H_2 does not occur on the Pt_2 cluster, at least in the side-on, on-top form and also in the side-on bridge form as we investigated.[3,30]

Another important aspect of the model study of chemisorption on a cluster surface is the stability of the cluster during catalytic processes. In order to examine it, we calculate the energy of point #13 in Figure 10, where the Pt_a-Pt_b distance is 5.492 Å, twice the original length of 2.746 Å, with the right H atom just above Pt_b. If any bonding remains between Pt_a and Pt_b after the migration of the H atom (#12), the energy of #13 would become higher than that of #12. However, the calculated results shown in Figure 14 indicate that the energy of #13 is almost the same as that of #12, implying that the Pt_a-Pt_b bond is completely broken after the hydrogen migration.

We thus conclude that the Pt_2 cluster does not react with the H_2 molecule and hence it is not a good model for chemisorption of a hydrogen molecule.

4.3. Pt_3-H_2 System

Here we examine, using a larger cluster Pt_3, the dissociative adsorption of an H_2 molecule and the migration of an H atom on a platinum surface. The reaction path is again the side-on, on-top approach shown in Figure 10 and all of the three Pt atoms Pt_a, Pt_b and Pt_c are involved. The geometries of the approach #1 - #12 are the same as those defined and used previously for the Pt-H_2 and Pt_2-H_2 systems. The results are shown in Figure 15.

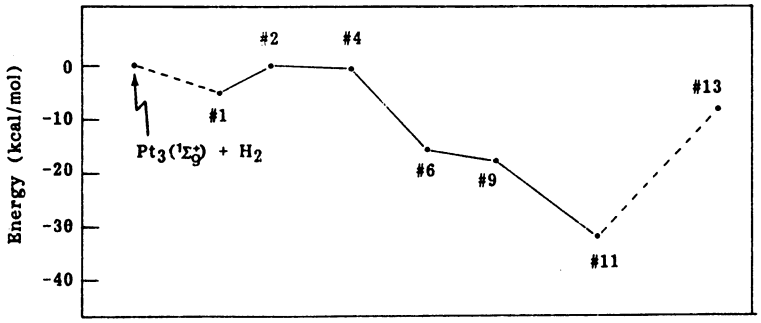

Figure 15. Potential energy diagram of the singlet A_1 state of the Pt_3-H_2 system calculated by the MC-SCF method.

The energy of #1 is lower than that of the free system, $Pt_3(^1\Sigma_g)$ + H_2 by 5.0 kcal/mol, probably indicating the physisorption state. At point #2, the system is

unstabilized by 4.7 kcal/mol in comparison with #1, but this is almost at the same level as the free system. The energy barrier which has to be overcome is considerably smaller in this system than in the previous Pt_2-H_2 system. At point #6, which is close to the most stable geometry of the Pt-H_2 system, the energy lowering from the free system is 15.7 kcal/mol. Although this is smaller than that of the Pt-H_2 system (about 40 kcal/mol), it is larger than that of the Pt_2-H_2 system (-21.9 kcal/mol). As the right H atom migrates on the Pt_3 surface from #6 to #11, the energy of the system is lowered again by 15.6 kcal/mol, with no energy barrier. The system prefers one H atom on each Pt atom rather than two H atoms on one Pt atom. The adsorption energy finally calculated for this system is 31.3 kcal/mol. This is obtained by substracting the energy of #11 from that of the free system $Pt_3(^1\Sigma_g)$ + H_2. This energy may be compared with the experimental adsorption energy, 24 kcal/mol of H_2 on a real Pt surface.[28]

We next examine the strength of the Pt-Pt bond during the migration process, as in the case of the Pt_2-H_2 system. At #13, the Pt_a-Pt_b distance is elongated to 5.492 Å, twice of the original distance, with the right H atom kept on Pt_b. The energy at #13 is higher than that at #11 by 23.3 kcal/mol, ensuring that even after the migration a reasonably strong bond exists between Pt_a and Pt_b. In contrast to the Pt_2 case, the stability of the Pt_3 cluster is related to the existence of the non-bonding σ MO which is considerably stabilized by the participation of the p_σ AO of the central Pt atom.

We thus conclude that the Pt_3 cluster reacts with the H_2 molecule as

$$\text{Pt-Pt-Pt} + \text{H}_2 \rightarrow \begin{matrix} & \text{H} & \text{H} \\ & | & | \\ \text{Pt-Pt-Pt} & & \end{matrix}$$

essentially without an energy barrier. This reaction gives a good model for actual surface reactions both in reproducing the adsorption energy and in showing the stability of the Pt-Pt bond during the dissociative adsorption process.

4.4. Short Summary

Thus, we have studied the reactions of a hydrogen molecule with small platinum clusters, Pt_n (n = 1,2,3). For the Pt_3 cluster, a linear geometry was assumed. We predict that the Pt atom and the Pt_3 cluster would react smoothly with H_2, but the Pt_2 cluster would not. The side-on on-top approach seems to be preferable. The catalytically active state of the Pt atom is not the ground $^3D(d^9s^1)$ state, but the excited $^1S(d^{10})$ state. In particular, the reaction with the Pt_3 cluster is suitable as a model of the hydrogen chemisorption on an actual platinum surface. The calculated heat of reaction was 40 kcal/mol (32 kcal/mol with including the spin orbit coupling) for the Pt-H_2 system, -12 kcal/mol for the Pt_2-H_2 system, and 32 kcal/mol for the Pt_3-H_2 system, in comparison with the experimental value, 26 kcal/mol for an extended surface.[28] The migration of H after dissociative adsorption occurs very smoothly without an energy barrier. The Pt-Pt bond of the Pt_3 cluster is stable during these processes. Experiments must now be undertaken on the reactivity of the small Pt clusters.

We summarize here the gross charges of the Pd_2H_2, PtH_2 and Pt_3H_2 systems

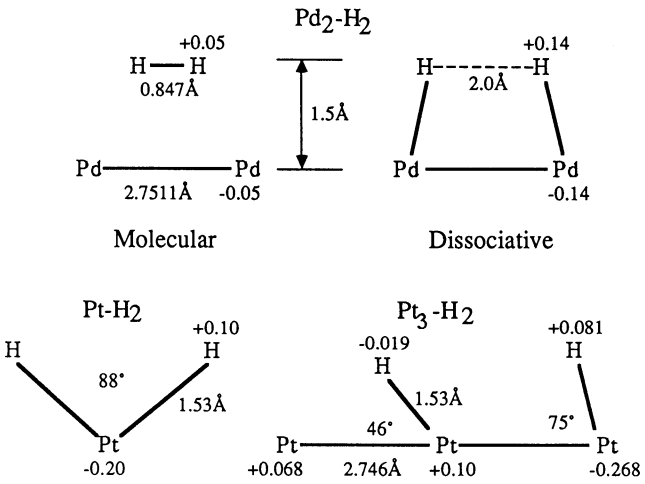

Figure 16. Geometries and gross charges of the Pd_2-H_2, Pt-H_2 and Pt_3-H_2 systems.

in Figure 16. The charges on the hydrogens are $+0.02 \sim +0.14$ which are small. Thus the electron transfers between the admolecules and the metal surfaces are small for hydrogen chemisorptions. This is why the cluster model is successful for describing the hydrogen chemisorptions on the Pd and Pt surfaces.

5. HYDROGEN CHEMISORPTION ON A ZnO SURFACE

Zinc oxide is an n-type semiconductor and has a catalytic activity for hydrogenations of olefins. It is a wultzite-type crystal and has many stable surfaces. It dissociatively adsorbs hydrogen molecule and the existence of some adsorbed hydrogen species is known.[31] Type I hydrogen shows a rapid and reversible adsorption and is responsible for the O-H and Zn-H IR peaks observed at 1710 and 3510 cm^{-1}, respectively.[32] This species is the principal source of hydrogens for the hydrogenation reaction of ethylene.[32] Type II hydrogen, on the other hand, contributes little to the hydrogenation of ethylene and does not give the Zn-H and O-H bands, but it promotes the rate of the catalytic reaction. Type III hydrogen exists at the temperature near 78 K. This is molecularly adsorbed on the same site as the type I species.[33]

On the theoretical side, some relevant papers have been published. In particular, Witko and Koutecky[34] studied the potential curves of ZnO + C_2H_4 and (ZnO + C_2H_4)$^+$ systems using the pseudo-potential MRD-CI and all electron MRD-CI methods. Attractive interactions have been found for several excited states of the ZnO + C_2H_4 system.

We have studied the hydrogen chemisorption on a ZnO surface.[4] The reaction path is calculated for the H_2 chemisorption on a ZnO surface. For simulating the ZnO(1010) surface, one ZnO molecule embeded in a Madelung potential is used. The ZnO distance is fixed at 1.95 Å, an experimental value for the crystal. The Madelung potential is expressed by the 32 point chargres of ± 0.5 situated on the first and second layers. The electrostatic potential due to the ionic layer decreases exponentially, so that the electrostatic potential made by the 32 point charges located around the ZnO

molecule reach to 92 % of the one due to 6886 point charges. The Madelung potential is proportional to the ionic charge, q, in $Zn^{+q}O^{-q}$. The Mulliken's atomic charge of ZnO calculated by the Hartree-Fock method is ± 0.6. However the smaller value should be used for q because of the electron spacial distribution. We then choose the point charge of ± 0.5.

5.1. ZnO

The potential curves of the low-lying states of an isolated molecule ZnO are calculated by the SAC/SAC-CI method. The results are shown in Figure 17. The ground state is $^1\Sigma^+$ for the Zn-O distance shorter than 1.98 Å, but at a larger distance the $^3\Pi$ state becomes the ground state. The equilibrium bond lenght of the $^1\Sigma^+$ state is 1.76 Å, which is shorter than the distance in the crystal, 1.95 Å. The bonding orbital is made of the 4s orbital of Zn and the 2pσ orbital of O. The binding energy is 20 kcal/mol and the dipole moment at the point of equilibrium is 5.82 Debye.

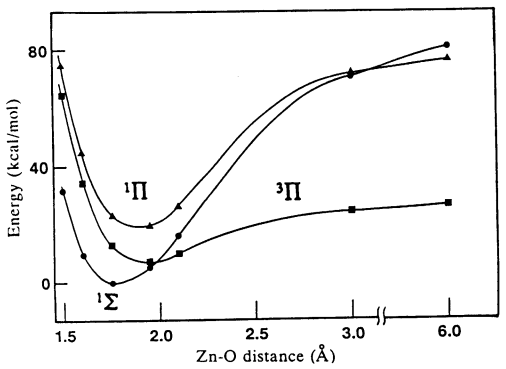

Figure 17. Potential energy curves for the lower singlet and triplet states of ZnO calculated by the SAC/SAC-CI method.

5.2. ZnO + H_2 System within the Madelung Potential

Figure 18 shows the reaction path for the hydrogen chemisorption on ZnO surrounded by the Madelung potential and the forces acting on the H atoms. The transition state exists between the points 3 and 4. The point 6 is the most stable geometry of this system. There, the H-H distance is 3.73 Å, which is 5 times as large as the one of a free H_2: namely, the H-H bond is completely broken. The H-Zn-O angle is 146°, in contrast to 180° obtained without the Madelung potential. The reason is the electrostatic repulsion between the adsorbed hydrogen and the surrounding Madelung potential. The H-O-Zn angle, on the other hand, is 111° which is slightly larger than 95° obtained without the Madelung potential.

The potential energies along the path calculated by the SAC/SAC-CI method are shown in Figure 19. We see that only the ground state is active for the hydrogen chemisorption. The reaction is exothermic by 73.5 kcal/mol and the reaction barrier is 11.5 kcal/mol. The Madelung potential lowers the barrier by 2.5 kcal/mol. The excited states are all repulsive. The calculated vibrational frequencies $\nu_{O\text{-}H}$ and

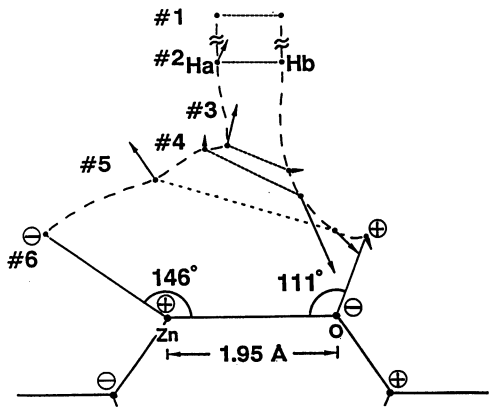

Figure 18. Forces acting on the H atoms in the ZnO + H_2 system with the Madelung potential.

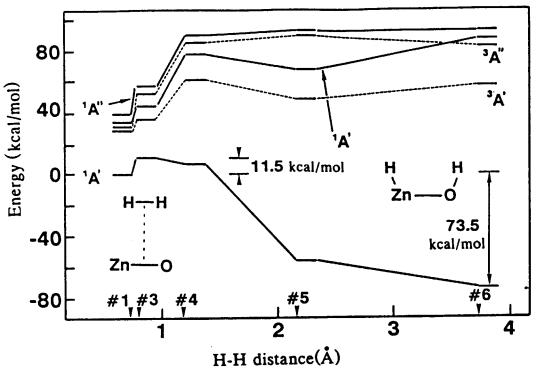

Figure 19. Potential energy diagram of the ground and several singlet and triplet excited states of the ZnO + H_2 system with the Madelung potential calculated by the SAC/ SAC-CI method.

νZn-H at the point 6 are 4090 and 1730 cm^{-1}, which are to be compared with the experimental values of 3510 and 1710 cm^{-1}, respectively.

Figure 20 shows the contour maps of the density difference defined by

$$\Delta\rho = \rho(ZnO - H_2) - \rho(ZnO) - \rho(H) - \rho(H) \quad (2)$$

At point 2, the density of H_2 is polarized by the long-range electrostatic dipole field of Zn^+O^-, so that the right-hand-side hydrogen becoms protonic. There is a large difference between the densities at 3 and 4, though there is a little difference in geometry between 3 and 4. It indicates that the transition state exists between 3 and 4. At 5, the H-H bond is completely broken, and the Zn-H and O-H bonds are formed. Along the Zn-H bond, the density on the left of the Zn-H bond increases and induces to the left the force acting on the hydrogen. Then this hydrogen moves and at 6, the final Zn-H and O-H bonds are formed. Throughout the reaction, the density in the ZnO region does not decrease, indicating that the Zn-O bond is kept stable. This is related to the stability of the catalytic surface.

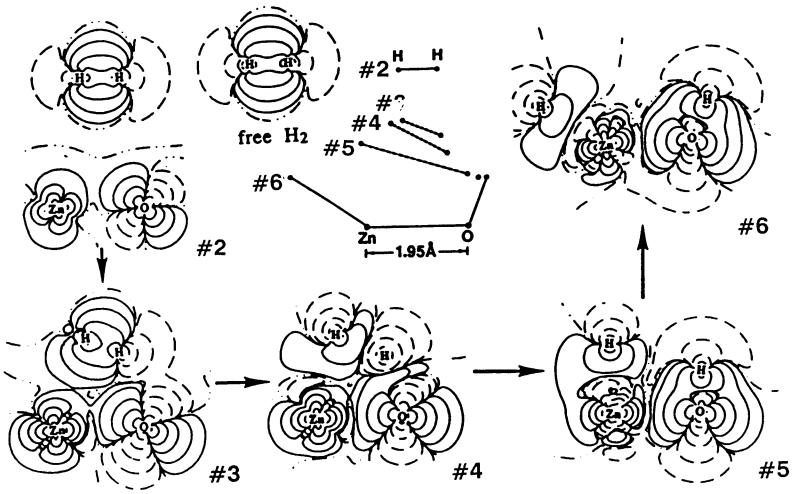

Figure 20. Reorganization of the electron density of the ZnO + H_2 system along the reaction path. The density difference is defined in the text.

5.3. Two Point Charges Plus H_2 System

Here, we study the role of the electrostatic polarization of ZnO for the reaction. To estimate the effect of the charges of ZnO on H_2, we replace Zn^+O^- by the two point charges (± 0.5) placed at the positions of Zn and O, and let H_2 approach along the reaction path shown in Figure 18. The energy is calculated by the full-CI method and given in Table I along with the atomic charges on H_a and H_b. We see that the electrostaic potential works to stabilize the system especially before reaching the barrier, namely the #3 geometry. It also considerably decreases the instability of the #4 and #5 geometries. The electrostaic polarization on ZnO induces a polarizatrion of the bonding σ_g MO of H_2 on the side of H_a (Figure 18) and the antibonding σ_u MO on the other side. This results in an increase of the overlaps between the σ_g orbital of H_2 and the LUMO of ZnO and between the σ_u orbital of H_2 and the $2p_\pi$ orbital of O. Thus, the electrostaic potential due to the charge polarization of Zn^+O^- makes the cleavage of H_2 easier.

Table I. Energies and atomic charges of H_2 along the reaction path where ZnO is replaced by the two point charges of ± 0.5. The energy of H_2 at the equilibrium bond length and without point charges is taken as a standard.

		with point charges		without point charges
			atomic charge	
point	$R_{H\text{-}H}$(Å)	ΔE(kcal/mol)	H_a/H_b	ΔE(kcal/mol)
2	0.7417	-0.19	-0.03/+0.03	0
3	0.7846	-10.23	0.00/0.00	0.69
4	1.2191	18.14	-0.05/+0.05	39.91
5	2.1674	43.36	-0.45/+0.45	97.70

5.4. Mechanism of the Reaction

The mechanism of this reaction is qualitatively explained as follows. The electron donation from the $2p_\pi$ orbital of O to the antibonding σ_u MO of H_2 and the backdonation from the bonding σ_g MO of H_2 to the LUMO of ZnO are important. In the initial stage of the reaction, the charge polarization of ZnO induces a polarization of the HOMO of H_2 on the side of Zn and LUMO on the side of O, which makes the electron transfer and back-transfer interaction with ZnO easier, because such a deformation of MO's increases the overlaps betwen the active MO's of H_2 and ZnO. Among the lower-lying states of ZnO, only the $^1\Sigma^+$ state (ground state) is catalytically active for the H_2 chemisorption. All the other low-lying states are repulsive. The Madelung potential enhaces the polarization of ZnO, namely Zn^+-O^-, and the reactivity with H_2 as a result. It also affect the geometry of the dissociatively adsorbed H_2 on a ZnO surface, and the energy gap between the ground and excited states. Throughout the reaction, another type of the $2p\pi$ orbital of O, which is parallel to the surface, and the bonding HOMO of ZnO is inactive and works to keep the ZnO bond stable during the catalytic process.

6. DIPPED ADCLUSTER MODEL (DAM) FOR CHEMISORPTIONS AND CATALYTIC REACTIONS ON A METAL SURFACE

In the previous sections we have used the cluster model for studying hydrogen chemisorptions and hydrogenation reactions on metal and metal oxide surfaces. A reason of the success is that the electron transfers between the admolecules and surfaces are small. Actually the gross charges of the admolecules in the hydrogen chemisorptions are shown in Figure 16. There, the charges on the admolecules are essentially neutral. However, when electron transfers between admolecules and surfaces are large, the cluster model may be inadequate, because the cluster itself has to supply or absorb electrons by much affecting the bondings within the cluster when the size of the cluster is small. In actual metal surfaces, a sufficient number of electrons are involved in the extended orbitals so that the transfer of electrons to or from the admolecule does not much affect the local bonding nature of the metal atoms of the cluster directly interacting with the admolecule. Thus, the cluster model would be incomplete for the surface reactions which accompany large electron (or spin) transfers between admolecules and bulk metals.

6.1. Dipped Adcluster Model (DAM)

We here propose a model for chemisorptions and surface reactions in which the electron transfers between admolecules and surfaces are large. We define 'adcluster' as a combined system of the admolecule and a cluster. We dip it onto the electron 'bath' of the solid metal and let an equilibrium be established for the electron and/or spin transfer between them. The equilibrium condition is described with the use of the chemical potentials of the adcluster and the solid surface. Namely, at equilibrium, the adcluster is at the $\min[E(n)]$ in the range,

$$-\frac{\partial E(n)}{\partial n} \geq \mu \tag{3}$$

where $E(n)$ is the energy of the adcluster with n being the number of electrons transferred from the bulk metal to the adcluster and μ the chemical potential of the electrons of the metal surface. Since the adcluster is a partial system, the number of the transferred electrons, n, is not necessarily an integer. In this model, the external effects such as those of promoters, cocatalysts, supports, temperature, electric potential, light, etc., are included through the variations of the chemical potential μ.

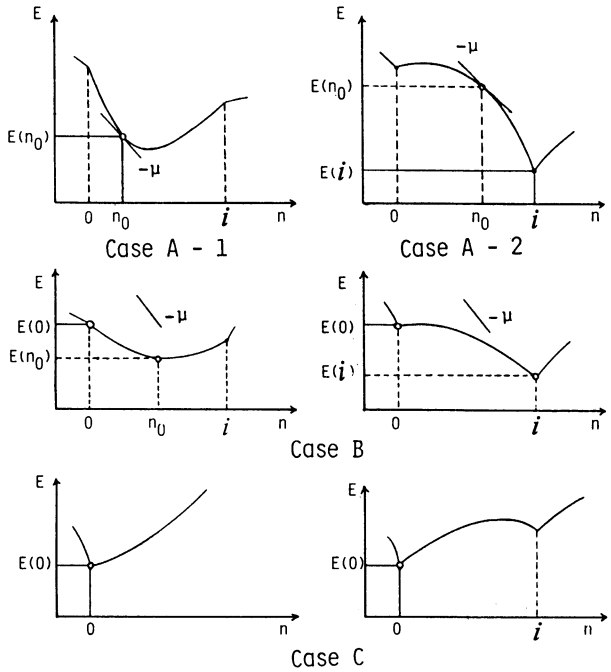

Figure 21. Some typical behaviors of the $E(n)$ curve as a function of n, the number of electrons transferred into the adcluster. On the horizontal axis, i denotes an integer number of electrons. The gradient μ is the chemical potential of the metal surface.

Some typical behaviors of the $E(n)$ curve are illustrated in Figure 21. In case A, the gradient becomes -μ at $n = n_0$. The $E(n)$ curve is lower and upper convexes in cases A-1 and A-2, respectively. The electrons flow into the adcluster up to n_0 and i in cases A-1 and A-2, respectively. We note that n_0 may be a non-integer but i is an integer. In case B, there is a region of n where $E(n)$ is lower than $E(0)$, but the gradient is smaller than μ in that region, so that the electron flow does not occur. A device for lowering μ is necessary for realizing the electron transfer. In case C, $E(0)$ is most stable in some wide region of n. In this case, the electron transfer can not be expected, so that the cluster model plus image force correction described below would be appropriate.

6.2. Molecular Orbital Model of the Dipped Adcluster

We give here molecular orbital model of the dipped adcluster and calculate the energy $E(n)$ and the electronic structure. We assume that the adcluster exchanges electrons and spins with the solid through its HOMO (highest occupied mo), LUMO (lowest unoccupied mo), SOMO (singly occupied mo), or some other active MO, with the

other MO's being doubly occupied or completely unoccupied. Such active MO is denoted by m. Two types of spin coupling are assumed for the electrons occupying the m-th MO. One is called highest spin coupling, in which the m-th MO is first occupied by α spin electron and after its occupation becomes equal to unity, it is then occupied by β spin electron. In this case, the adcluster is paramagnetic. The other is paired spin coupling in which the same amounts of α and β spin electrons occupy the m-th MO. Here, the adcluster is diamagnetic. The energy of the adcluster with x electrons occupying the m-th MO, which is assumed to be non-degenerate, is given by

$$E^{(0)} = 2\sum_k H_k + \sum_{k,l}(2J_{kl} - K_{kl}) + x\sum_k(2J_{km} - K_{km}) + x\,H_m + Q \quad (4)$$

where k, l run over the doubly occupied MO's. H_k, J_{kl} and K_{kl} denote core-hamiltonian integral, coulomb repulsion integral, and exchange repulsion integral, respectively. The meaning of the superscript (0) will be self-evident later. The quantity Q represents the electron repulsion within the active orbital m and depends on the nature of the spin coupling as described above. It is given by

$$Q = \| x - 1 \| \; J_{mm} \quad (5a)$$

for the highest spin coupling and

$$Q = (\frac{x}{2})^2 \; J_{mm} \quad (5b)$$

for the paired spin coupling. Here, $||a|| = 0$ if $a < 0$, $||a|| = a$ if $0 \leq a \leq 1$, and $||a|| = 1$ if $a > 1$. It is easy to prove that Q is minimum for the highest spin coupling and maximum for the paired spin coupling. Therefore, the energy of the adcluster itself is lowest in the highest spin coupling. The actual preference of the way of the spin coupling would also depend on the nature of the solid and of the interaction between the adcluster and solid. For example, when some amount of α spin is transferred from the solid metal to the adcluster, the system is spin polarized and paramagnetic near the adcluster. For cases in which the orbital m is degenerate, see ref. 1.

The energy of the open-shell restricted Hartree-Fock (RHF) method is written as

$$E = \sum_k \lambda_k H_k + \frac{1}{2}\sum_k\sum_l \lambda_k\lambda_l(\alpha_{kl}J_{kl} - \beta_{kl}K_{kl}). \quad (6)$$

By a comparison between Eqs.(6) and (4), the occupation parameter λ_k and the spin coupling parameters α_{kl} and β_{kl} in Eq.(6) are fixed, so that performing the RHF-MO SCF calculation involving the non-integral occupation number x, we obtain the molecular orbitals and the energy $E(x)$.

6.3. Electrostatic Image Force

When an adatom A at the position a has a charge q, it induces an opposite charge on a metal surface. At point $\mathbf{x}(x, y, 0)$ of the surface, the induced charge density is given by,[35]

$$\sigma(\mathbf{x}) = -\frac{q|\mathbf{a} - \mathbf{a}'|}{4\pi|\mathbf{a} - \mathbf{x}|^3} \tag{7}$$

where $\mathbf{a}'$ is the positional vector of the mirror image of the adatom A. The electrostatic interaction between the charge q and the hole $\sigma(\mathbf{x})$ sums up to the well-known image force given by

$$\mathbf{F}_{if} = \int\int_{xy}^{\text{surface}} \frac{\sigma(\mathbf{x})q}{|\mathbf{a} - \mathbf{x}|^3}(\mathbf{a} - \mathbf{x})dxdy = \frac{q^2(\mathbf{a}' - \mathbf{a})}{|\mathbf{a} - \mathbf{a}'|^3}, \tag{8}$$

and the stabilization energy is given by

$$E_{if} = \int\int_{xy}^{\text{surface}} \frac{\sigma(\mathbf{x})q}{2|\mathbf{a} - \mathbf{x}|}dxdy = -\frac{q^2}{2|\mathbf{a}' - \mathbf{a}|} \tag{9}$$

where the factor 2 in the denominator is due to the integration over the half space ($z \geq 0$). For polyatomic systems, see ref. 1.

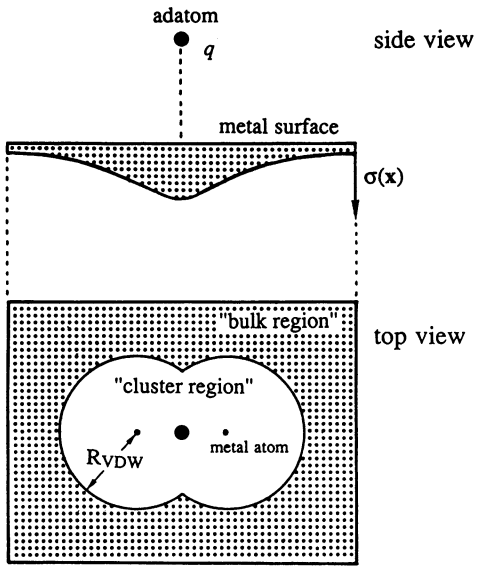

Figure 22. Schematic representation of the adatom and the induced charge density on the surface. The cluster region is estimated from the Van der Waals radius of the metal atom.

When the energy $E^{(0)}$ of the adcluster alone is calculated by an ab initio method, the electrostatic interaction within the adcluster is already included. Therefore, the electrostatic term $E^{(1)}$ is estimated, as illustrated in Figure 22, by integrating the electrostatic interaction between the charge q and the hole $\sigma(\mathbf{x})$ at the point $\mathbf{x}$ outside the cluster region of the surface. In practice, the energy $E^{(1)}$ is calculated by subtracting from E_{if} the electrostatic energy (E_{in}) for $\sigma(\mathbf{x})$ inside the cluster region, that is,

$$E^{(1)} = E_{if} - E_{in}. \tag{10}$$

As sketched in Figure 22, the cluster region of the surface is estimated by the Van der Waals radius of the metal atom, and the Mulliken's atomic charge is used for q.

The energy of the system thus becomes,

$$E = E^{(0)} + E^{(1)} \tag{11}$$

where $E^{(0)}$ is the energy of the adcluster alone and $E^{(1)}$ the energy of the electrostatic interaction between the adcluster and the bulk metal.

The estimation of the electrostatic energy may be done before or after MO calculations. In principle, the effect should be included before MO calculations because, then, we can include the relaxation of the electron cloud of the adcluster in the electrostatic field of the surface. Since q and $\sigma(\mathbf{x})$ depends on each other, the calculations are done iteratively. We have shown in the previous paper[1] that these two methods give very similar results. Therefore, we here calculate the image force correction after MO calculations.

6.4. Palladium-O_2 System

We apply the dipped adcluster model to palladium-O_2 system, representing a palladium surface by a single Pd atom. The O_2 molecule is put at end-on, on-top position of the Pd atom, so that the adcluster is a linear Pd-O_a-O_b system. At an infinite separation, the O_2 molecule is in the $^3\Sigma_g$ state and the Pd atom is in the $^1S(d^{10})$ state. We first apply the highest spin coupling model and then the paired spin coupling model. Though the former gives a continuous picture leading to the correct separation limit, the latter does not. The electrons are transferred into the degenerate π^* MO's of the PdO_2 system from the Pd solid.

6.4.1. Highset Spin Coupling

Figure 23 is a display of the $E(n)$ curve, the energy of the adcluster calculated as a function of n, the number of the electrons transferred into the adcluster. This figure is for the Pd-O_a distance fixed at 2.0 Å, which is almost the most stable distance. The O-O distance is changed from 1.20752 Å, which is an equilibrium length R_{eq} of O_2,[19] to 1.35 Å, which is an equilibrium length of O_2^-,[19] and further to 1.5 Å. The chemical potential of the solid palladium metal is 5.12 eV,[36] which is shown by the gradient in Figure 23. Clearly, the behavior of the curves corresponds to Case A-2. Therefore, after some barrier, one electron flows from the bulk metal into the adcluster, so that the adcluster becomes $(Pd\text{-}O_2)^-$. The energy of this charged state is lower than that of the neutral one.

Figure 24 shows the potential energy curve for the end-on approach of the O_2 molecule to the palladium surface. The broken lines are for $E^{(0)}$ alone and the solid lines for $E^{(0)} + E^{(1)}$. The broken and solid curves for $n = 0.0$ nearly overlap each other, since the electrostatic term is very small. The broken curve for $n = 0.0$ corresponds to the cluster model, which results in that the O_2 molecule is not adsorbed onto Pd in contrary to the experiment. This result also shows that a linear PdO_2 molecule does not exist. On the other hand, when the electron transfer from the bulk metal to the adcluster is admitted, the system becomes stable as O_2 approaches Pd, which is shown by the broken curve of $n = 1.0$. Furthermore, the image force term is also important for stabilizing the system as shown by the solid curve of $n = 1.0$.

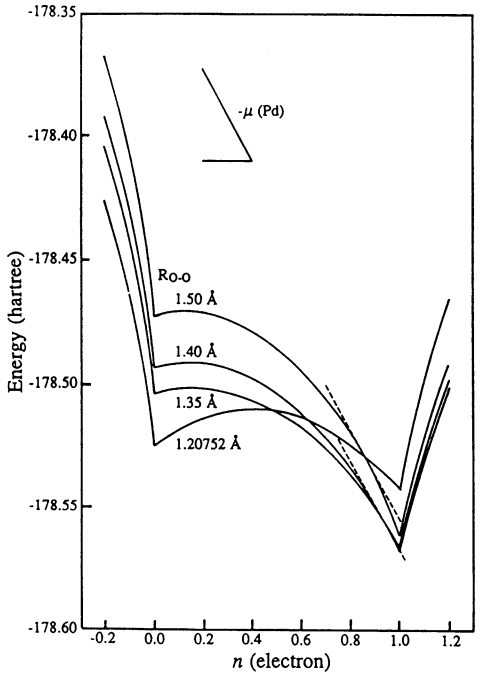

Figure 23. $E(n)$ curves for the Pd-O_a-O_b system in the highest spin coupling model with the O-O distances of 1.20752, 1.35, 1.40, and 1.50 Å and the Pd-O_a distance fixed at 2.00 Å.

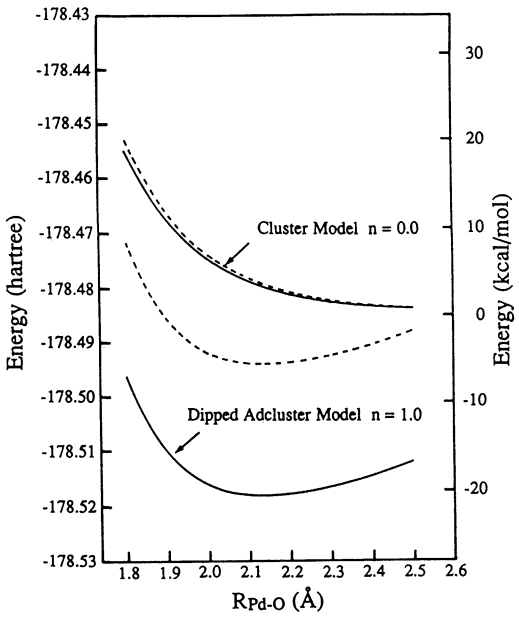

Figure 24. Potential energy curves for the end-on approach of the O_2 molecule onto palladium calculated by the highest spin coupling. The O-O length is fixed at 1.20752 Å (equilibrium length of the free O_2) for the upper one and at 1.35 Å for the lower one. Broken and solid lines are calculated, respectively, without and with the electrostatic energies $E^{(1)}$. The upper broken line with $n = 0.0$ corresponds to the cluster model. The energy scale on the right-hand side is in kcal/mol relative to the free Pd plus O_2 system.

Table II. The adsorption energy, geometry, and vibrational frequency of the PdO_2 adcluster in the highest spin coupling model.

	adsorption energy [a]	bond length (Å)		vibrational frequency (cm^{-1})	
	(kcal/mol)	$R_{Pd\text{-}O}$	$R_{O\text{-}O}$	$\omega_{Pd\text{-}O}$ [b]	$\omega_{O\text{-}O}$
$E^{(0)}$ alone	6.4	2.15	1.39	329	1229
$E^{(0)} + E^{(1)}$	21.9	2.15	1.40	338	1250
experiment	7.6 ~12.3		1.32±0.05 [c]	485 [c]	1035

[a] Relative to the HF energy of Pd (^1S) + O_2 ($^3\Sigma_g^-$); -178.48500 hartree.
[b] O_2 is assumed to vibrate as a unit.
[c] For O_2 on a Pt(111) surface.

Table II shows a summary of the adsorption energy and some geometrical and vibrational parameters. It also shows the effect of the image force. For the adsorption energy, the effect of $E^{(1)}$ is large but for the geometrical and vibrational parameters, it is very small, since the image force is a long-range force. The agreement between theory and experiment is reasonable, considering the simplicity of the theoretical model. Probably the effect of $E^{(1)}$ is overestimated here since the adcluster is too small in this calculation.

The Mulliken population at the optimal geometry is Pd(-0.186)-O_a(-0.584)-O_b(-0.236). The inner O_a atom is more negatively charged than the outer O_b atom. However, the frontier orbital of this adcluster has largest amplitude on the outer O_b atom, so that the O_b atom is expected to be more reactive than the O_a atom.

6.4.2. Paired Spin Coupling

The $E(n)$ curves calculated for the paired spin coupling model are displayed in Figure 25. The curves are lower convexes in contrast to the upper ones of Figure 23. At n = 0.25, the tangent of the curve for R(O-O) = 1.35 Å coincides with the chemical potential $-\mu$ of the solid palladium metal 5.12 eV,[36] and the adcluster is the most stable there in the range defined by Eq.(3). Therefore, about 0.25 electron flows into the adcluster from the bulk metal; thus, the adcluster has a non-integer number of electrons. When the chemical potential μ of the metal is regulated, for example, by an external potential, the number of electrons n transferred into the adcluster are regulated. At the limit of μ = 0.0, about 1.15 electrons flow into the adcluster, which corresponds to the minimum of the $E(n)$ curve for R(O-O) = 1.40 Å.

Figure 26 shows the potential energy curves for the Pd-O distance for the Pd-O_2 adcluster with fixed n of 0.25, though of course, the number of electrons n should be optimized as the functions of these distances. Broken and solid lines are calculated respectively without and with the image force term $E^{(1)}$. The geometries and the vibrational frequencies of the adsorbed system are calculated from these curves and shown in Table III. They are similar to the results of the highest spin coupling model shown in Table II, though the bond lengths of the Pd-O and O-O bonds calculated by the paired spin coupling model are a little shorter than those by the highest spin coupling model, and the force constants are a little larger. A reasoning for these

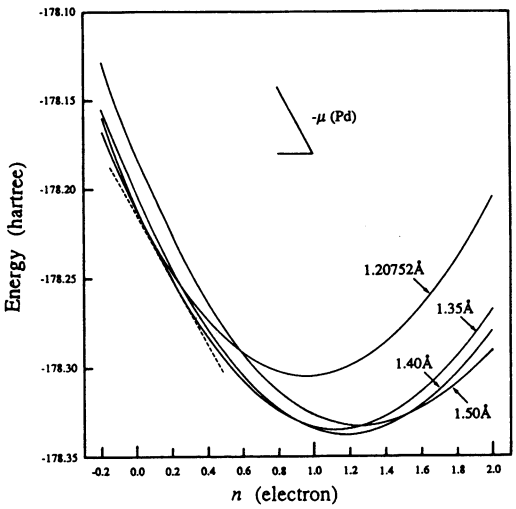

Figure 25. $E(n)$ curves for the Pd-O_a-O_b system in the paired spin coupling model with the O-O distances of 1.20752, 1.35, 1.40, and 1.50 Å and the Pd-O_a distance fixed at 2.00 Å.

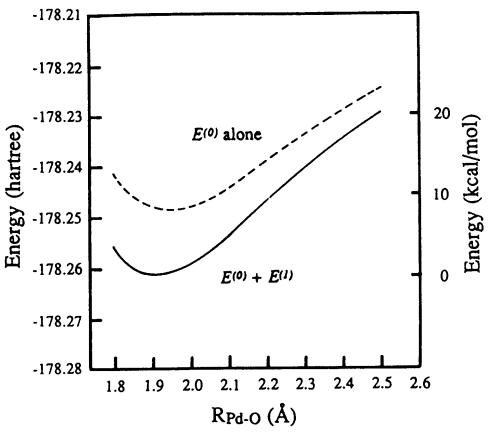

Figure 26. Potential energy curves for Pd-O vibration calculated by the paired spin coupling. The O-O length is fixed at 1.35 Å. Broken and solid lines are calculated, respectively, without and with the electrostatic energies $E^{(1)}$.

small differences is given in ref. 1.

The Mulliken's atomic charge of the adcluster is Pd(+0.301)-O_a(-0.349)-O_b(-0.202). The charge on Pd is positive, which we think more reasonable than the previous result of the highest spin coupling. The inner oxygen O_a is again more negative than the outer O_b atom.

6.5. Brief Remarks

Here, we have explained the dipped adcluster model for the study of chemisorptions and catalytic reactions on a metal surface which involve large electron transfer between an admolecule and a metal surface. The size of the cluster necessary for investigating such electronic processes would be reduced if the dipped adcluster model is adopted instead of the conventional cluster model. This merit is practically very

Table III. Geometry and vibrational frequency of the PdO_2 adcluster calculated by the paired spin coupling model.

	bond length (Å)		vibrational frequency (cm^{-1})	
	$R_{Pd\text{-}O}$	$R_{O\text{-}O}$	$\omega_{Pd\text{-}O}$ [a]	$\omega_{O\text{-}O}$
$E^{(0)}$ alone	1.96	1.30	389	1259
$E^{(0)} + E^{(1)}$	1.93	1.31	399	1279
experiment		1.32±0.05 [b]	485 [b]	1035

a) O_2 is assumed to vibrate as a unit.
b) For O_2 on a Pt(111) surface.

important since electron correlations are often very important for describing the model reactions on cluster surfaces and further since sometimes the catalytically active state is not necessarilly the ground state but an excited state of the surface cluster. We therefore have to make the size of the cluster as small as possible. Although we have restricted the present formulation only within the molecular orbital model, an inclusion of electron correlation is necessary. Further, it is interesting to investigate the effect of the cluster size on the dipped adcluster model. If the size is large enough to be able to describe the real surface, the dipped adcluster model would, in principle, become unnecessary. But, how large is such size ?

7. MOLECULAR AND DISSOCIATIVE CHEMISORPTIONS OF AN O_2 MOLECULE ON AN Ag SURFACE

Partial oxidation of ethylene on a silver surface is an important catalytic reaction, for which no catalysts except for silver have been found effective.[37] However, the mechanism of this catalytic reaction is not yet completely elucidated. We do not yet understand why only a silver surface has such a reactivity and selectivity.

Experimentally, four different species are known for the adsorbed oxygens on a silver surface;[38-44] namely, physisorbed species (O_2),[38] molecularly adsorbed species, which are superoxide (O_2^-)[39,40] and peroxide (O_2^{2-}),[40-43] and dissociatively adsorbed species (O^- or/and O^{2-}).[41,44]

Some theoretical papers have been published on the oxygen chemisorptions.[45-50] The GVB-CI study by Upton et al.[47] gave geometric and spectroscopic parameters of O_2 on an Ag surface in good agreement with the experimental data. However, the molecular adsorption energies relative to the ground state were not reproduced: they were negative. Carter et al.[48] reported an extensive study on the mechanism of the partial oxidation of ethylene on a silver surface. All of these studies used the cluster model, so that the effects of the bulk metal are only insufficiently included in the calculations. So far, no ab initio studies have been able to describe the dissociative adsorption of an O_2 molecule on an Ag surface, though recently Panas et al.[49] have successfully described the O-O dissociation on a nickel surface.

We have applied the DAM for studying the mechanism of the chemisorption of an oxygen molecule on a silver surface. Figure 27 shows the $E(n)$ curve for the

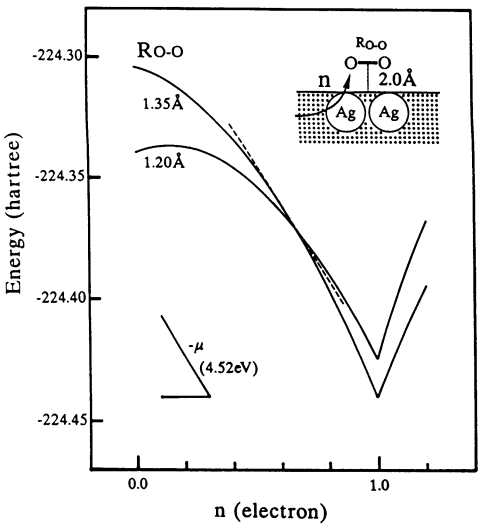

Figure 27. $E(n)$ curves for the Ag_2-O_2 adcluster in the highest spin coupling model with the Ag_2-O_2 distance of 2.00 Å and the Ag-Ag distance of 2.8894 Å.

Ag_2O_2 adcluster in the highest spin coupling model. The geometry is shown in the figure. The Ag-Ag distance is fixed to 2.8894 Å, the lattice distance in a crystal. The curve is A-2 type, so that one electron transfer from the bulk metal into the adcluster is expected. For surface electronic processes involving transition metals, electron correlations are often quite essential. Since we are going to study several different adsorption states of O_2, we have to calculate several lower states of the system. Sometimes, the catalytically active state is not necessarily the ground state of the system. For this purpose, we use the SAC/SAC-CI method which is proved to be very accurate and useful for studying ground, excited, ionized, and electron-attached states of a molecule.[7-10] Since Figure 27 shows only one-electron transfer is important in this case, we can calculate the correlated wave functions of this system by the SAC/SAC-CI method.

7.1. Approach of O_2 onto a Silver Surface

We first show the energetics for the approach of an O_2 molecule onto an Ag surface. The active site of an Ag surface is represented by Ag_2, and an O_2 molecule approaches the surface in a side-on bridge form keeping C_{2v} symmetry. This geometry was suggested by Backx et al. for O_2 adsorbed on an Ag(110) surface.[42] Figure 28 shows the potential energy curves of the Ag_2O_2 adcluster calculated by the SAC/SAC-CI method as a function of the Ag_2-O_2 distance. The curves are calculated for the O-O distance fixed at 1.35 Å, which is an equilibrium distance of an O_2 anion.[47] The asterisks show the energies at the optimized O-O distances.

The $^3B_2$ state, which does not involve an electron transfer from the bulk metal to the adcluster, is the ground state of the separated system; namely, the $^1\Sigma_g$ state of Ag_2 and the $^3\Sigma_g$ state of O_2. The energy of the dissociation limit is estimated by optimizing the O-O distance at the Ag_2-O_2 distance of 5.0 Å, and is shown by the

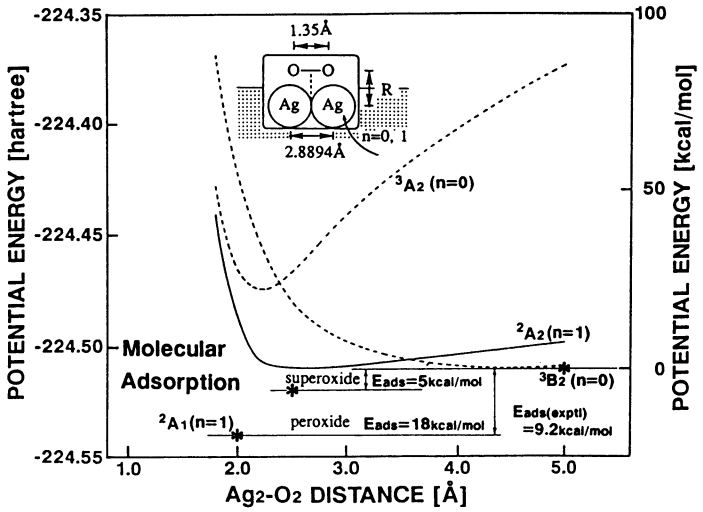

Figure 28. Potential energy curves for the approach of O_2 onto Ag_2 in the Ag_2-O_2 adcluster. n denotes the number of the electrons transferred from the bulk metal to the adcluster.

asterisk in Figure 28. There, the optimized O-O length is 1.29 Å, in comparison with 1.27 Å, the optimized length for the free O_2 molecule (the experimental value is 1.207 Å[50]). The potential curve for the $^3B_2$ state rises monotoniously as O_2 approaches Ag_2, showing that no chemisorption occurs along this state.

When one electron transfer is admitted from the bulk metal to the adcluster, namely $n = 1$, the potential of the $^2A_2$ state becomes attractive and a minimum is found at $R(Ag_2\text{-}O_2) = 2.6$ Å. When the O-O distance is further optimized at this minimum, we get R(O-O) = 1.50 Å and the system is stabilized down to the asterisk shown in Figure 28. This $^2A_2$ state corresponds to the superoxide species, O_2^-. There is another state, $^2A_1$ state, which also results from the one-electron transfer from the bulk metal to the adcluster. This $^2A_1$ state corresponds to the peroxide species, O_2^{2-}, and has a potential minimum at $R(Ag_2\text{-}O_2) = 2.0$ Å and R(O-O) = 1.66 Å. The corresponding energy is shown by the asterisk in Figure 28. The calculated adsorption energies of the superoxide and peroxide species are 5.5 and 17.8 kcal/mol, respectively, in comparison with the experimental molecular adsorption energy of 9.2 kcal/mol.[43]

The $^3A_2$ state shown in Figure 28 is an electron transferred state from Ag_2 to O_2, but no electron is supplied from the bulk metal ($n = 0$). The image force term is included and works to stabilize the system. Though the system is stabilized as O_2 approaches the surface, the energy is always higher than the free molecule limit. This state corresponds to the molecularly adsorbed species obtained by the conventional cluster model and the adsorption energy is negative as in the previous studies.[47] This failure is mainly due to a limitation of the cluster model. In the cluster model, all the electrons transferred to O_2 must be supplied from Ag_2, but in DAM some of the electrons are supplied from the bulk metal. We see that the

electron transfer from the bulk metal to the adcluster is essential for the occurrence of the chemisorption of an O_2 molecule on an Ag surface. We have confirmed that the stabilization of the charged O_2 admolecule by the electrostatic image force of the Ag metal is also important.

7.2. Potential Curve for O-O Stretching and Dissociation on an Ag Surface

Figure 29 shows the potential energy curves for the O-O elongation on the Ag_2 site. These potentials are calculated for the Ag_2O_2 adcluster with $n = 1$ with fixing the Ag_2-O_2 distance at 2.0 Å. As before, the $^2A_2$ and $^2B_1$ states correspond to the superoxide species and the $^2A_1$ state to the peroxide species. These potentials are calculated by the SAC/SAC-CI method.

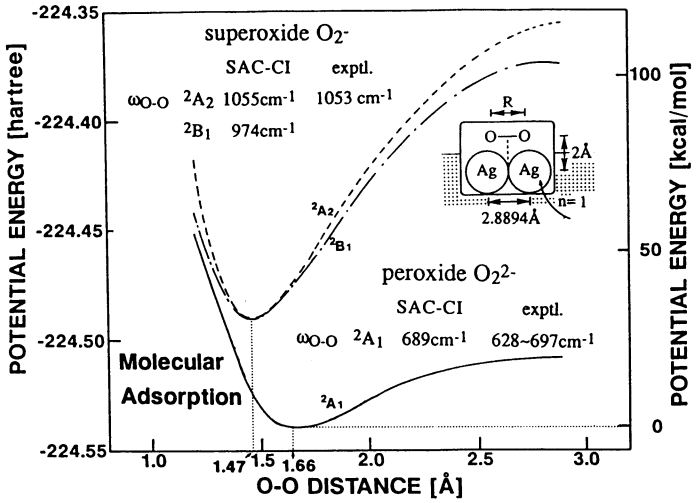

Figure 29. Potential energy curves for the O-O elongation in the Ag_2-O_2 adcluster.

The equilibrium adsorption geometries and the vibrational frequencies of the superoxide and peroxide are calculated and shown in Table IV. The calculated vibrational frequencies agree well with the experimental values. The calculated O-O distance of the peroxide is larger than the experimental one. The gross charge of superoxide is calculated to be $O_2^{-0.5 \sim -0.6}$ and that of peroxide as $O_2^{-1.4}$, which are smaller than the formal charges in the notations O_2^- and O_2^{2-}, respectively. Backx et al. estimated the charge of -1.7 for peroxide from the consideration on the vibrational frequency as a function of the number of electrons in the π^* antibonding orbitals.[42]

It is expected that the dissociative adsorption is led from the peroxide species ($^2A_1$), because the curves of the superoxide species ($^2A_2$, $^2B_1$) rise more rapidly than that of the peroxide as the O-O distance is elongated. However, the potential curve of the peroxide rises monotonically up to R(O-O) = 2.8894 Å, which is twice

Table IV. The adsorption geometries and vibrational frequency of the molecular adsorption species of O_2 on an Ag surface.

Species	State	Bond Length (Å) R(Ag_2-O_2)	Bond Length (Å) R(O-O)	O-O Vibrational Frequency (cm^{-1})
superoxide	$^2A_2$	2.6	1.47	1055
	$^2B_1$	—	1.47	974
	exptl.	—	—	1053
peroxide	$^2A_1$	2.0	1.66	689
	exptl.	—	1.47 ± 0.05	628 ~ 697

as large as the O-O distance of the free O_2 molecule. We could not obtain the second minimum corresponding to the dissociatively adsorbed state from the calculations for the Ag_2O_2 adcluster. A reason is attributed to the electrostatic repulsion between the negative charges on oxygens. It is estimated as large as 60 kcal/mol from the gross charges on the oxygens (-0.72) separated by 2.8894 Å. For realizing the stabilization of the dissociative state, two oxygen atoms must be separated further on the surface. We, therefore, need a larger surface of the Ag atoms, so that we next consider the dissociation of O_2 on the linear Ag_4.

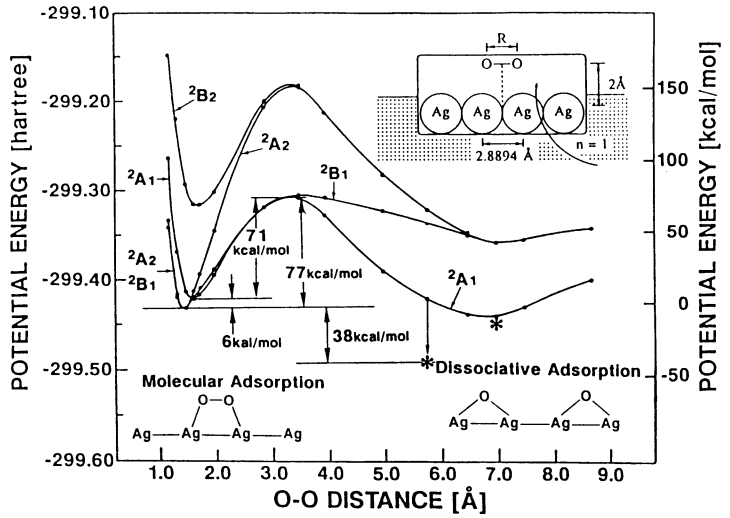

Figure 30. Potential energy curves against the O-O distance for the Ag_4-O_2 adcluster.

Figure 30 shows the potential energy curves for the ground and excited states of the Ag_4O_2 adcluster with $n = 1$. They are again due to the SAC/SAC-CI calculations. In contrast to the calculations for the Ag_2O_2 adcluster, we here have frozen the electron correlations of the d-orbitals of the silvers. In Figure 30, we get the

potential minima of not only the molecular adsorption states ($^2A_1$, $^2A_2$, and $^2B_1$) near R(O-O) = 1.5 Å, but also the dissociative adsorption state ($^2A_1$) at R(O-O) = 7.0 Å. When we further optimize the Ag_4-O_2 distance at R(O-O) = 5.7788 and 7.0 Å, it becomes shorter up to 1.60 and 1.90 Å, respectively, and the corresponding energies are shown by the asterisks in Figure 30. The system is most stable at R(O-O) = 5.7788 Å, and R(Ag_4-O_2) = 1.60 Å. The dissociated oxygens are adsorbed at the two-fold bridge site of the Ag surface, as illustrated in Figure 30, and the Ag-O length is calculated to be 2.16 Å, which agrees with the observed distance of 2.06 ~ 2.17 Å.[46] The gross charge of oxygen at the optimized geometry is -0.98 and so the dissociated oxygen is essentially O^-.

Table V. Adsorption energies of O_2 on a silver surface. (kcal/mol)

Adsorption State		Theoretical	Experimental	
			Ag(110)	Ag(111)
molecular	superoxide	5.5	9.3	9.2
	peroxide	17.8		
dissociative		44.0 61.4	42.5	39.9

The dissociative adsorption state is lower by 38.5 and 43.6 kcal/mol than the molecular superoxide and peroxide species, respectively. By the thermal desorption spectra of O_2 adsorbed on Ag(111) and Ag(110),[45] the dissociative adsorption state is observed to be lower by 31.6 and 34.7 kcal/mol, respectively, than the molecular adsorption state. We summarize the calculated and experimental adsorption energies in Table V. The energy barrier between the molecular and dissociative adsorptions lies at R(O-O) = 3.5 Å, with the height of 77.2 kcal/mol from the superoxide species and 71.2 kcal/mol from the peroxide species. This barrier may be too large, in comparison with that in Figure 29, and this may be attributed to the neglect of the correlations of the d electrons for the Ag_4O_2 adcluster. The reorganization of the Ag surface would also work to reduce the barrier.

ACKNOWLEDGEMENT

The authors thank Prof. T. Yonezawa, Mr. Y. Matsuzaki, and Y. Fukunishi for collaborations in some of the studies included in this review. The calculations have been carried out at the computer centers of the Institute for Molecular Science and of Kyoto University. Parts of these studies have been supported by the Grant-in-Aids for Scientific Research from the Ministry of Education, Science, and Culture of Japan.

REFERENCES

[1] H. Nakatsuji, J. Chem. Phys., **87**, 4995 (1987); H. Nakatsuji, H. Nakai, and Y. Fukunishi, J. Chem. Phys., **95** , 640 (1991).

[2] H. Nakatsuji, M. Hada, and T. Yonezawa, J. Am. Chem. Soc., **107**, 8264 (1985); **109**, 1902 (1987).
[3] H. Nakatsuji, Y. Matsuzaki, and T. Yonezawa, J. Chem.Phys., **88**, 5769 (1988).
[4] H. Nakatsuji and Y. Fukunishi, Intern. J. Quantum Chem., in press.
[5] H. Nakatsuji, M. Hada, and T. Yonezawa, Surface Sci., **185**, 319 (1987).
[6] H. Nakatsuji, H. Nakai, Chem. Phys. Letters, **174**, 283 (1990).
[7] H. Nakatsuji and K. Hirao, J. Chem. Phys., **68**, 2035 (1978).
[8] H. Nakatsuji, Chem. Phys. Letters, **59**, 362 (1978); **67**, 329, 334 (1979); Chem. Phys. **75**, 425 (1983).
[9] H. Nakatsuji, Program System for SAC and SAC-CI calculations, Program Library No. 146 (Y4/SAC), Data Processing Center of Kyoto University (1985); Program Library SAC85, No. 1396, Computer Center of Institute for Molecular Science (1986).
[10] H. Nakatsuji, Report in Molecular Theory, CRC Press, in press.
[11] (a) P. J. Hay, J. Am. Chem. Soc., **103**, 1390 (1981); (b) J. O. Noell and P. J. Hay, Inorg. Chem., **21**, 14 (1982). (c) P. J. Hay and W. R. Wadt, J. Chem. Phys., **82**, 270 (1985).
[12] (a) S. Huzinaza, J. Chem. Phys., **42**, 1293 (1965); (b) T. H. Dunning Jr., ibid **53**, 2823 (1970).
[13] (a) H. Nakatsuji, K. Kanda, and T. Yonezawa, Chem. Phys. Letters, **75**, 340 (1980); (b) H. Nakatsuji, T. Hayakawa, and M. Hada, Chem. Phys. Letters, **80**, 94 (1981); (c) H. Nakatsuji, K. Kanda, H. Hada, and T. Yonezawa, J. Chem. Phys., **77**, 3109 (1981).
[14] T. H. Dunning, Jr. and P. J. Hay, "Modern Theoretical Chemistry", edited by H. F. Schaeffer III, Plenum, New York, 1977, Vol.3.
[15] B. R. Brooks, P. Saxe, W. D. Laidig and M. Dupuis, Program System GAMESS; Program Library No.481, Computer Center of the Institute for Molecular Science, (1981).
[16] R. C. Weast, Ed. "Handbook of Chemistry and Physics", CRC Press, Cleveland, 1984–1985, F-167.
[17] (a) B. Roos, P. Taylor, and P Siegbahn, Chem. Phys., **48**, 157 (1980); (b) P. Siegbahn, A. Heiberg, B. Roos, and B. Levy, Phys. Scr., **21**, 323 (1980)
[18] (a) H. Conard, G. Ertl, and E. E. Latta, Surface Sci., **41**, 435 (1974); (b) R. J. Behm, K. Christmann, and G. Ertl, Surface Sci., **99**, 320 (1980); (c) C. Nyberg and G. C. Tengstal, Surface Sci., **126**, 163 (1983).
[19] K. P. Huber and G. Herzberg, "Molecular Spectra and Molecular Structure. IV. Constants of Diatomic Molecules" Van Nostrand Reinhold Co., New York, 1979.
[20] (a) C. F. Melius, Chem. Phys. Letters, **39**, 287 (1976); (b) C. F. Melius, J. W. Moskowitz, A. P. Mortola, M. B. Baillie, and M. A. Ratner, Surface Sci., **59**, 279 (1976).
[21] W. Eberhardt, S. G. Louie, and E. W. Plummer, Phys. Rev., **B28** 465 (1983).
[22] J. P. Muscat, Surface Sci., **148**, 237 (1984).
[23] N. A. Baykara, J. Andzelm, S. Z. Baykara, and D. R. Salahub, Intern. J. Quantum Chem., **29**, 1025 (1986).
[24] (a) G. C. Bond, D. A. Dowden, and N. Mackenzie, Trans. Faraday Soc. **54** 1537 (1958). (b) G. C. Bond and P. B. Wells, J. Catal., **4**, 211 (1965); **5** 65, (1965).
[25] R. B. Woodward and R. B. Hoffmann, "The Conservation of Orbital Symmetry", Academic Press, New York, 1970.
[26] G. Henrici-Olive and S. Olive, "Coordination and Catalysis", Verlag Chemie: Weinheim, 1977.
[27] G. C. Bond, "Catalysis by Metals" Academic Press, New York, 1962.
[28] J. R. Anderson, "Structure of Metallic Catalysts", Academic, New York, 1975.
[29] C. E. Moore, "Atomic Energy Levels", National Bureau of Standards, Washington, D. C., 1971, vol. 3
[30] H. Nakatsuji and M. Hada, Croat. Chem. Acta, **57**, 1371 (1984).

[31] R. P. Eischens, W. A. Pliskin, and M. J. D. Low, J. Catal., **1**, 80 (1962); R. Ugo, Catal. Rev., **11**, 225 (1975).
[32] A. L. Dent and R. J. Kokes, J. Phys. Chem., **73**, 3781 (1969).
[33] W. C. Conner, Jr. and R. J. Kokes, J. Catal., **36**, (1975).
[34] M. Witko and V. B. Koutecky, Intern. J. Quantum Chem., **24**, 1535 (1986).
[35] J. H. Jeans, "The Mathematical Theory of Electricity and Magnetism", chapter VIII, Cambridge University, New York (1966).
[36] H. B. Michaelson, J. Appl. Phys., **48**, 4729 (1977).
[37] A. Ayame and H. Kanoh, Shokubai **20** 381 (1978) in Japanese.
[38] D. Schmeisser, J. E. Demuth and Ph. Avouris, Phys. Rev., **B26** 4857 (1982).
[39] K. C. Prince and A. M. Bradshow, Surface Sci., **126** 49 (1983).
[40] C. Pettenkofer, I. Pockrand and A. Otto, Surface Sci., **135**, 52 (1983); C. Pettenkofer, J. Eickmans, U. Erturk and A. Otto, Surface Sci., **151**, 9 (1985).
[41] (a) A. Sexton and R.J. Madix, Chem. Phys. Letters **76**, 294 (1980). (b) M. A. Bartreau and J. Madix, Chem. Phys. Letters, **97**, 85 (1983).
[42] C. Backx, C. P. M. deGroot and P. Biloen, Surface Sci., **104**, 300 (1981); C. Backx, C. P. M. deGroot, and P. Biloen, Appl. Surface Sci., **6**, 256 (1980).
[43] D. A. Outka, J. Stohr, W. Jark, P. Stevens, J. Solomon and R. J. Madix, Phys. Rev. **B35**, 4119 (1987); J. Stohr and D. A. Outka, Phys. Rev., **B36**, 7891 (1987).
[44] C. T. Campbell, Surface Sci., **157**, 43 (1985).
[45] J.-H. Lin and B. J. Garrison, J. Chem. Phys., **80**, 2904 (1984).
[46] A. Selmani, J. Andzelm, and D. R. Salahub, Intern. J. Quantum Chem., **29**, 829 (1986).
[47] T. H. Upton, P. Stevens, and R. J. Madix, J. Chem. Phys., **88**, 3988 (1988).
[48] E. A. Carter and W. A. Goddard III, Surface Sci., **209** 243 (1989).
[49] I. Panas, P. Siegbahn and U. Wahlgren, J. Chem. Phys., **90**, 6791 (1989).
[50] P. H. Krupenie, J. Phys. Chem. Ref. Data 1 423 (1972).